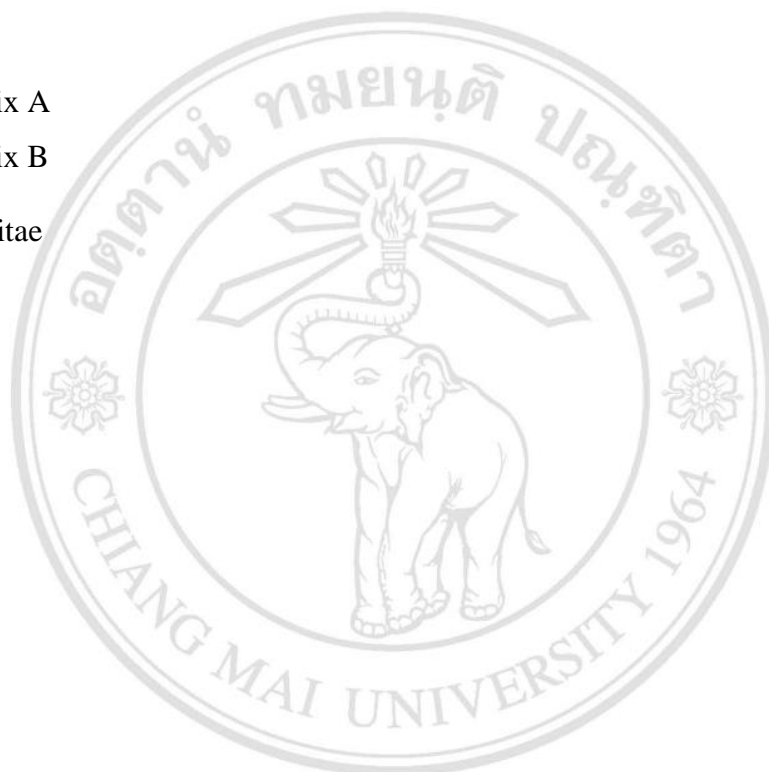


CONTENTS

	Page
Acknowledgement	d
Abstract in Thai	f
Abstract in English	h
List of Tables	m
List of Figures	n
List of Symbols	q
Chapter 1 Introduction	1
1.1 Catalyst	1
1.2 Catalysis on semiconductors	1
1.3 Photocatalysis	6
1.4 Redox reaction in photocatalysis	6
1.5 Enhancement of photocatalysis	8
1.6 Model of heterogeneous catalysis	8
1.7 Steps in heterogeneous reactions	9
1.8 Physical adsorption and chemisorption	10
1.9 Kinetics of heterogeneous catalytic reactions	11
1.10 Catalyst deactivation	12
1.11 Heterojunction	13
1.12 The effect of bad edge on pH of electrolyte solution	15
1.13 Theoretical predictions of the position of band edges	19
1.14 Organic pollutant	20
1.15 Synthesis methods for semiconductor photocatalysts	22
1.16 Reviews	26
1.17 Aim and scope of this study	35
1.18 Usefulness of the research (Theoretical and/or Applied)	36

References	37
Chapter 2 Experiment	42
2.1 Materials	42
2.2 Instruments	43
2.3 Sample Preparation	44
2.4 Sample characterizations	45
2.4.1 X-ray diffraction (XRD)	45
2.4.2 Scanning electron microscope (SEM)	46
2.4.3 Ultraviolet-visible spectroscopy (UV-vis spectroscopy)	48
2.4.4 Photocatalytic activity test	51
2.4.5 Photoluminescence (PL)	52
2.4.6 Fourier-transform Infrared Spectroscopy (FTIR)	55
2.4.7 Brunauer Emmett Teller method (BET)	57
2.4.8 X-ray fluorescence Analysis (XRF)	60
2.4.9 Energy Dispersive X-ray analysis (EDX)	62
2.4.10 X-ray photoelectron spectroscopy (XPS)	63
2.4.11 Transmission Electron Microscopy (TEM)	64
References	66
Chapter 3 Results and Discussion	69
3.1 Characteristic properties of photocatalysts	70
3.1.1 X-ray diffraction (XRD) characterization	80
3.1.2 Scanning electron microscope (SEM)	75
3.1.3 Photocatalytic testing	77
3.1.4 UV-vis diffuse reflectance spectroscopy (UV-vis DRS)	79
3.1.5 Brunauer Emmett Teller method (BET)	82
3.1.6 Fourier-transform Infrared Spectroscopy (FTIR)	83
3.1.7 Transmitting electron microscope (TEM)	85
3.1.8 Photoluminescence (PL)	85
3.1.9 X-ray fluorescence analysis (XRF)	86

3.2 The band alignment investigation by XPS technique and proposed energy diagram with charge transferring	88
3.3 The role of individual component and the main active species in heterostructure system	92
References	99
Chapter 4 Conclusion	103
Appendix	105
Appendix A	105
Appendix B	110
Curriculum Vitae	113



ลิขสิทธิ์มหาวิทยาลัยเชียงใหม่
 Copyright© by Chiang Mai University
 All rights reserved

LIST OF TABLES

	Page
Table 1.1 Comparison between homogeneous and heterogeneous catalysis	6
Table 1.2 Differences between physical adsorption and chemisorption interaction	11
Table 1.3 Comparison on the main characteristic features between α -phase and β -phase of Ag_3VO_4	27
Table 1.4 A summary of synthesis methods for Ag_3VO_4	29
Table 1.5 A summary of synthesis methods of CoTiO_3 .	30
Table 2.1 Chemicals, Molecular weight, Purity, and Company	42
Table 2.2 Degrees of freedom for polyatomic molecules	56
Table 3.1 Details on XRD patterns of CoTiO_3 and Ag_3VO_4 for calculation of cell parameters and unit cell volume of each constituent materials	73
Table 3.2 Size comparison between the calculated crystallite size from XRD and particle size from SEM measurement of each component	76
Table 3.3 A summary of the absorption edge and the calculated band gap energy of different $\text{Ag}_3\text{VO}_4/\text{CoTiO}_3$ coupling systems	80
Table 3.4 Comparison of the BET SSAs of each catalysts	82
Table 3.5 Stretching and bending modes of Ag_3VO_4 and CoTiO_3 with their corresponding wave numbers	83
Table 3.6 Elemental analysis of composite material of 50% $\text{Ag}_3\text{VO}_4/\text{CoTiO}_3$ from XRF measurement	87
Table 3.7 XPS CL peaks and VBM positions used to calculate the VBO of $\text{Ag}_3\text{VO}_4/\text{CoTiO}_3$ heterojunction	91
Table 3.8 Scavenger added for the specific active species trapping	95

LIST OF FIGURES

	Page
Figure 1.1 E-k diagram of direct	2
Figure 1.2 Broaden band energy level of overlapped outer atoms of solid	3
Figure 1.3 Continuous band energy	4
Figure 1.4 Band energy diagram of intrinsic semiconductors and extrinsic semiconductors of n-type and p-type doping	5
Figure 1.5 Redox reaction in photocatalysis from the view point of water splitting reaction for the evolution of H ₂ and O ₂ molecules	7
Figure 1.6 Energy band diagram for a uniform semiconductor	13
Figure 1.7 Band alignment of type I heterojunction	14
Figure 1.8 Band alignment of type II heterojunction	15
Figure 1.9 Band alignment of type III heterojunction	15
Figure 1.10 Schematic energy model of the n-type semiconductor/electrolyte interface	16
Figure 1.11 Schematic view of the electric double layers at the n-type semiconductor/aqueous electrolyte interface with corresponding potential distributions	17
Figure 1.12 Simplified scheme of the protonation and deprotonation of hydroxylated TiO ₂ surface leading to positive and negative net charge at the surface	18
Figure 1.13 Structure of methylene blue	20
Figure 1.14 Absorption spectra of methylene blue	20
Figure 1.15 Concentration of the solute before and after nucleation	25
Figure 1.16 Structure of monoclinic α -Ag ₃ VO ₄	27
Figure 1.17 Structure of Ilmenite CoTiO ₃	30
Figure 1.18 Schematic diagram of synergistic effect of Co ₃ O ₄ /Ag ₃ VO ₄	33
Figure 1.19 Proposed degradation mechanism of Ag ₃ VO ₄ /TiO ₂ system	34

Figure 1.20	Comparison of PL spectra and proposed electron–hole transfer mechanism at the NiTiO ₃ /Ag ₃ VO ₄ interface	35
Figure 2.1	Bragg’s law reflections	45
Figure 2.2	The process of electron interaction with the electron in atomic sample	42
Figure 2.3	The schematic of SEM technique	42
Figure 2.4	The path length of electron penetration	48
Figure 2.5	Schematic of band gap measurement by UV-vis DRS	50
Figure 2.6	Photocatalytic set up in the black box	52
Figure 2.7	Partial Jablonski Diagram for Absorption, Fluorescence, and Phosphorescence	52
Figure 2.8	Schematic of PL characterization	54
Figure 2.9	Radiative recombination paths	54
Figure 2.10	Changes in the dipole moment of a heteronuclear diatomic molecule	55
Figure 2.11	Carbon dioxide and water molecules	56
Figure 2.12	Brunauer’s classification of adsorption isotherm	60
Figure 2.13	Lay out of XRF	61
Figure 2.14	Schematic representation of an energy-dispersive spectrometer	62
Figure 2.15	Interaction between electrons and the sample	65
Figure 2.16	Schematic of light transmission in the TEM instrument	65
Figure 3.1	X-ray diffraction patterns of obtained materials and their corresponding JCPDS files.	70
Figure 3.2	FWHM estimation from XRD pattern to calculate crystallite size of CoTiO ₃	72
Figure 3.3	FWHM estimation from XRD pattern to calculate crystallite size of Ag ₃ VO ₄	72
Figure 3.4	Surface morphology of Ag ₃ VO ₄ , CoTiO ₃ , composite and the EDS spectrum of composite	75
Figure 3.5	The formation of rod-like CoTiO ₃ via sol-gel method by using ethylene glycol as a solvent	77
Figure 3.6	Photocatalytic MB degradation activities under visible light irradiation	78

Figure 3.7	The plot between $\ln(C/C_0)$ and irradiation time (min)	79
Figure 3.8	The plot between Kubelka-Munk absorbance and light irradiation wavelength of Ag_3VO_4 , CoTiO_3 and composites	80
Figure 3.9	Splitting of free-ion F and P terms in octahedral and tetrahedral fields	82
Figure 3.10	Infrared transmittance band of each constituent and theirs composite	84
Figure 3.11	TEM images of CoTiO_3 (a) and composite (b) with the lattice fringes related to (104) plane of CoTiO_3	85
Figure 3.12	Photoluminescence study of pure Ag_3VO_4 , pure CoTiO_3 and composite system upon laser excitation at 345 nm	86
Figure 1.13	XPS CL of pure Ag_3VO_4 , 50% $\text{Ag}_3\text{VO}_4/\text{CoTiO}_3$, pure CoTiO_3 and the VB spectra of each constituents.	90
Figure 3.14	Band alignment corresponding to type-II heterojunction and the proposed charge transfer diagram of $\text{Ag}_3\text{VO}_4/\text{CoTiO}_3$ system	91
Figure 3.15	The light cut-off ranges by yellow ($\lambda < 510$ cut off) and red ($\lambda < 585$ cut off) filter	93
Figure 3.16	MB degradation activity of photocatalysts with and without filter for 3 h irradiation	93
Figure 3.17	Proposed charge transfer of coupling system between $\text{Ag}_3\text{VO}_4/\text{CoTiO}_3$ under normal light condition, under yellow filter, and red filter	94
Figure 3.18	Effect of active species scavenger on the photoactivity of the individual components and hybrid system	95
Figure 3.19	Fluorescence emission spectra of 2-hydroxy terephthalic acid obtained from Ag_3VO_4 , CoTiO_3 and the coupling system	98

LIST OF SYMBOLS

β	The peak width measured at half height measured in radius
BE	Electron binding energy
BET	Brunauer-Emmett-Teller
c	Speed of light
C_t	Concentration at time
C_0	Initial concentration
d	the lattice planar spacing or thickness
BE	Binding energy
E_F	Fermi level
E_g	Optical band gap of the semiconductor
E_{CB}	Conduction band energy
E_{VB}	Valence band energy
h	Plank's constant (6.63×10^{-34} J.s), hour
$h\nu$	Photon energy
h^+	Hole
I_0	Intensity of the incident beam
I	Intensity of the transmittance
IEP	Isoelectric point
IUPAC	International Union of Pure and Applied Chemistry
JCPDS	Joint Committee Powder Diffraction Standards
K	Absorption coefficient
KE	Kinetic energy
MB	Methylene blue
SHE	Standard hydrogen electrode
p	Pressure at the constant temperature
p_0	Saturation pressure at the measurement temperature
SEM	Scanning Electron Microscopy

BSE	backscattering electron
SSA	Specific Surface Area
T	Transmittance
TEM	Transmission Electron Microscopy
t	Time
UV-Vis	Ultraviolet-Visible
VB	Valence band
CB	Conduction band
VBM	Valence band maximum
CBM	Conduction band minimum
VBO	Valence band offset
CBO	Conduction band offset
CL	Core level
XPS	X-ray photo-electron spectroscopy
XRD	X-ray diffraction
Z	Atomic number
λ	Wavelength
λ_{edge}	Wavelength at absorption edge
Φ	Work function
ε	Molar absorptivity
V	Volume
V_m	Volume of gas adsorbed
θ	The Bragg angle for the reflection
ν	Frequency

ลิขสิทธิ์ © โดย Chiang Mai University
All rights reserved